Article

Dual-Metal Zeolitic Imidazolate Framework Derived Highly Ordered Hierarchical Nanoarrays on Self-Supported Carbon Fiber for Oxygen Evolution

Xi Du [1,2,*], Wenjun Zhang [1,2], Maliang Zhang [1,2], Yanhong Ji [1,2], Kunmei Su [1,3] and Zhenhuan Li [1,2,*]

1   State Key Laboratory of Separation Membranes and Membrane Processes, Tiangong University,
    Tianjin 300387, China; zhangwenjun970716@163.com (W.Z.); zhangmaliang@tiangong.edu.cn (M.Z.);
    jiyanhong@tiangong.edu.cn (Y.J.); sukunmei@tiangong.edu.cn (K.S.)
2   School of Materials Science and Engineering, Tianjin Key Laboratory of Advanced Fibers and Energy Storage,
    Tiangong University, Tianjin 300387, China
3   School of Chemistry and Chemical Engineering, Tiangong University, Tianjin 300387, China
*   Correspondence: duxi@tiangong.edu.cn (X.D.); lizhenhuan@tiangong.edu.cn (Z.L.);
    Tel.: +86-022-83955358 (Z.L.)

Abstract: The construction of highly ordered hierarchical nanoarrays is crucial for obtaining effective transition metal carbon nanomaterial electrocatalysts for oxygen evolution reaction (OER) in water splitting. Herein, we adopted a Co metal zeolitic imidazolate framework (Co-ZIF) as a precursor by ion-exchange/etching reaction with $Fe(NO_3)_3$ to obtain hierarchical N-doped Co-Fe layered double hydroxide (CoFe-LDH) in situ generated in Co-ZIF nanoarrays based on a self-supported carbon cloth (CC) substrate noted as CoFe-LDH@Co-ZIF@CC. Benefiting from the synergistic effect of these species and their highly ordered self-supported nanoarray structure, the catalytic active sites were fully exposed and highly protected in alkaline electrolyte, which significantly promoted electron transport and improved electrochemical performance. The CoFe-LDH@Co-ZIF@CC exhibited the low overpotentials of about 225 and 319 mV at 10 and 100 mA cm^{-2} with a small Tafel slope of 81.8 mV dec^{-1} recorded in a 1.0 M KOH electrolyte. In addition, it also showed a long-term durability without obvious decay after 30 h. Therefore, its remarkable OER activity demonstrates this material's promising application in the green hydrogen energy industry.

Keywords: zeolitic imidazolate framework; layered double hydroxide; hierarchical nanoarrays; self-supported; synergistic effect

1. Introduction

Renewable energy could be the dominant form of energy use in future societies, of which hydrogen energy has received increasing attention due to its high energy density, cleanliness and sustainability [1–3]. Electrochemical water splitting provides an attractive approach for the production of pollution-free and high-purity hydrogen energy [4]. However, this technology still faces problems, such as its low energy efficiency, high overpotential and poor stability [5,6]. This is mainly due to the inefficient oxygen evolution reaction (OER) derived from sluggish four-electron transfer, which is the major bottleneck of the water splitting [7]. Currently, commercial Ir- or Ru- based catalysts are expensive, have poor stability and are rare, which have severely hampered their widespread use. Thus, to explore and develop highly efficient and cheap non-noble-metal electrocatalysts is the key to solving the above problem.

Traditionally, carbon materials such as graphene or carbon nanotubes have been an alternative to precious metals [8]. Currently, transition-metal carbon nanomaterials, on account of their high reserves, low cost, excellent catalytic activity and environment-friendly features have become well-respected OER electrocatalyst materials, and can be

used as an alternative to noble-metal catalysts [2,9]. Transition metals represented by Fe and their compounds have proven to be extremely effective OER catalysts [10]. For example, a previous study used a Fe^{3+} ion-assisted aniline polymerization strategy to embed bimetallic CoFeP nanospheres into the nitrogen-doped porous carbon framework, and excellent OER performance was recorded [11]. In other previous studies, zeolitic imidazolate framework (ZIF) materials with advantages such as a high porosity, extremely high nitrogen contents and adjustable structure have been used as a kind of important precursor for preparing N-doped transition metal carbon nanomaterial [12,13]. These materials usually have large specific surface areas, abundant active sites and various pore structures, which are particularly advantageous for electrocatalytic processes. However, many related reports have inevitably revealed a serious problem of catalyst aggregation at the micro level, resulting in buried catalytic active sites that are deeply unexposed, which is more unbeneficial for facilitating the OER. Simultaneously, most powdered catalysts need to be combined with a polymer binder for preparing the electrode, and this will significantly block the active sites and increase the interface resistance, making it difficult to meet the requirements for the high efficiency and stability of electrochemical water splitting. Thus, using ZIF as a precursor to in situ construct a self-supported electrode with a well-organized three-dimensional (3D) skeleton on a conductive fabric is an effective way to improve the electron transfer/penetration ability.

In addition, the catalytic effect of a single type of metal is limited, and the introduction of different types of metals to achieve bimetal synergy is an effective means [14]. Nevertheless, achieving a high degree of fusion between the doped metal and the precursor matrix is still a challenging task. Layered double hydroxide (LDH) has the commonly used formula of $[M^{2+}_{1-x} M^{3+}_x (OH)_2] (A^{n-})_{x/n} \cdot mH_2O$, where M^{3+} and M^{2+} represent trivalent and bivalent metal cations, and A^{n-} represents the charge-balancing anion [15]. It takes a tremendous effort to prepare LDH with the transformation of ZIF to introduce additional metal ions. For example, Nie and his coworkers reported a method to fabricate NiFe-LDH nanosheets derived from ZIF-67 in situ grown on nickel foam, which significantly improved the catalytic performance of the OER [16]. Xu and his coworkers integrated a 2D ZIF-67 nanoarray and ternary LDH CoNiAl to obtain the hierarchical ZIF-67/CoNiAl-LDH/NF electrocatalyst, which displays outstanding OER activity, having a low overpotential of 303 mV at 10 mA cm^{-2} [17]. As a result, this is an effective strategy to adjust the electronic structure distribution of the original substance, and gives full play to the synergistic effect of bimetals in order to better improve the electrocatalytic performance.

Inspired by the above considerations, we adopted Co-ZIF as a precursor by ion-exchange/etching reaction with $Fe(NO_3)_3$ to obtain the hierarchical N-doped Co-Fe LDH in situ generated in the Co-ZIF nanoarrays based on a self-supported carbon cloth (CC) substrate, which was noted as CoFe-LDH@Co-ZIF@CC. Owing to the inherent synergistic effect among these species, CoFe-LDH@Co-ZIF@CC displayed superior OER activity. When applied in a KOH electrolyte, CoFe-LDH@Co-ZIF@CC not only showed low overpotentials of 225 and 319 mV at 10 and 100 mA cm^{-2} current density, but also presented excellent durability. These results demonstrate this material's promise as an application in the green hydrogen energy industry.

2. Experimental Section

2.1. Preparation of Co-ZIF@CC

Firstly, 0.58 g $Co(NO_3)_2 \cdot 6H_2O$ was immersed in 40 mL aqueous solution and poured in 40 mL aqueous solution containing 1.31 g of 2-methylimidazole at room temperature. Then, a piece of 3×5 cm^2 CC was chosen and acidized and immersed in the mixed solution for 8 h. After that, above CC was washed 3 times and dried at 100 °C for 8 h to achieve Co-ZIF@CC.

2.2. Preparation of CoFe-LDH@Co-ZIF@CC

A total of 0.18 g of $Fe(NO_3)_3 \cdot 9H_2O$ was dissolved in 50 mL absolute ethanol, and one piece of Co-ZIF@CC (1×3 cm^2) was soaked in the solution and slowly stirred for 1 h. Then, the sample was dried at 70 °C for 8 h to achieve CoFe-LDH@Co-ZIF@CC.

2.3. The Loading of the CoFe-LDH@Co-ZIF@CC and Co-ZIF@CC Catalyst

In order to calculate the quality of Co-ZIF@CC and CoFe-LDH@Co-ZIF@CC, the synthetic Co-ZIF@CC was weighed and then soaked in 1 M HCl for ultrasound for 30 min. Then, it was removed and washed with distilled water until it was neutral. After drying, it was weighed again. Since Co-ZIF@CC would react with HCl, the mass lost was the loading of Co-ZIF@CC. The mass loading of CoFe-LDH@Co-ZIF@CC was also calculated in the same way. Finally, the calculated mass loading of Co-ZIF@CC and CoFe-LDH@Co-ZIF@CC was found to be about 2 mg cm^{-2}.

2.4. The Loading of Commercial IrO$_2$@CC

As the comparison material, the loading of commercial IrO$_2$@CC was required to be the same as that of CoFe-LDH@Co-ZIF@CC and Co-ZIF@CC. Thus, the commercial IrO$_2$@CC catalyst was prepared by dropping IrO$_2$ dispersion liquid mixture, and the quality difference of the electrode before and after dropping was 2.0 mg cm^{-2}, which was the quality of IrO$_2$.

3. Results and Discussion

As illustrated in Figure 1, the synthesis route of CoFe-LDH@Co-ZIF clearly exhibited uniformly hierarchical nanoarrays on the self-supported CC substrate. Firstly, the acidized CC substrate was placed into a water solution mixture of $Co(NO_3)_2 \cdot 6H_2O$ and 2-methylimidazole at room temperature to achieve leaf-like Co-ZIF@CC nanoarrays as a sacrificial template. Subsequently, Fe^{3+} ions were successfully introduced into the Co-ZIF@CC by ion exchange/etching process to achieve Co-Fe LDH (noted as CoFe-LDH@Co-ZIF@CC) to synergistically improve the catalytic capacity. The hierarchical nanoarrays of these materials were investigated by scanning electron microscopy (SEM). As we can see from Figure 2a,b, Co-ZIF@CC nanosheets created a fascinating hierarchical structure, with uniformly and smoothly triangular shape surfaces grown on the CC substrate. The SEM images of the CoFe-LDH@Co-ZIF@CC in Figure 2c,d show that its structural integrity was maintained well without collapse and aggregation after the ion exchange/etching process. When carefully observed, it can be seen that the overall surface arrays were quite rough with some evident "wrinkles". It is beneficial to obtain more electroactive sites [12]. We further tested the sample for HRTME (Figure S3), and in the inset Figure 2d, the interplanar distance of 0.26 nm lattice fringe corresponds to CoFe-LDH (012).
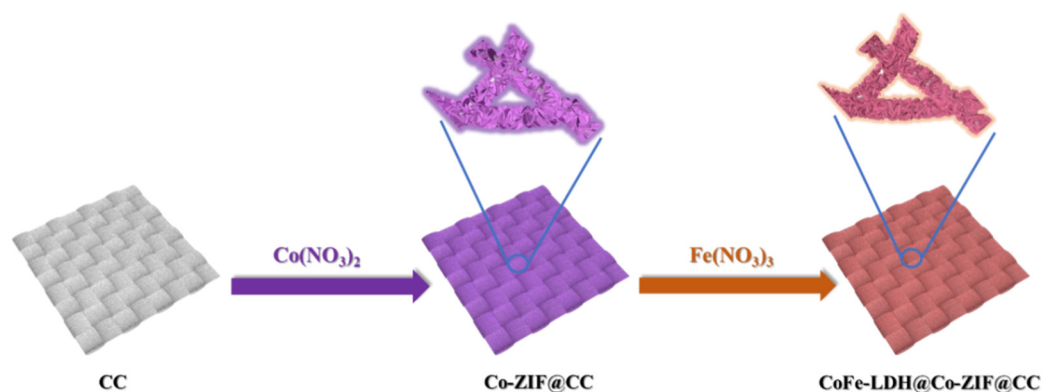
Figure 1. Synthesis route of hierarchical CoFe-LDH@Co-ZIF@CC electrode.
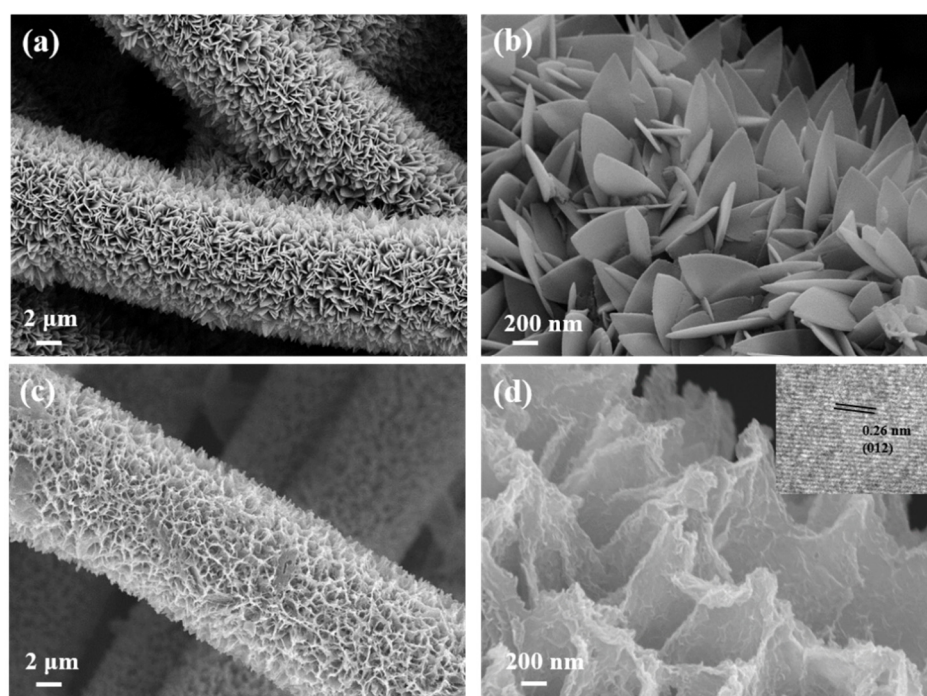
Figure 2. SEM images of (**a**,**b**) Co-ZIF@CC and (**c**,**d**) CoFe-LDH@Co-ZIF@CC (inset: the lattice image).

The crystalline phase purity and conversion of the as-prepared CoFe-LDH@Co-ZIF@CC and Co-ZIF@CC samples were investigated by XRD. All the samples exhibited characteristic peaks at ~25° and ~43° corresponding to the interlayer spacing (002) and the plane spacing (100) of graphite carbon, respectively (Figure 3a). For Co-ZIF@CC, the strong characteristic peaks ranging from 12~18° were consistent with the reported Co-L-ZIF (Figure S4), indicating its high purity. After the ion exchange/etching process, the XRD for the CoFe-LDH@Co-ZIF@CC showed new diffraction peaks at about 11.5°, corresponding to the (003) plane of CoFe-LDH (JCPDS No. 50-0235), which implies that this formed the composite CoFe-LDH and Co-ZIF. Because the crystallinity of CoFe-LDH was weak and overlapped with the peaks of Co-ZIF and CC, only the (003) side of CoFE-LDH was observed [18]. Raman spectra of both samples exhibited two typical peaks from 1357 and 1592 cm^{-1} (Figure 3b) corresponding to the D and G bands, which indicated that there exists both defects and graphitization [19]. The ratio of I_D/I_G of CoFe-LDH@Co-ZIF@CC was 1.01, larger than that of Co-ZIF@CC (0.99), indicating that there were more defects in CoFe-LDH@Co-ZIF@CC.

To further investigate the elements and valence states of the CoFe-LDH@Co-ZIF@CC catalyst, X-ray photoelectron spectroscopy (XPS) was used. As displayed in Figure S5 and Table S1, the survey spectrum of CoFe-LDH@Co-ZIF@CC demonstrated that the Co, Fe, O, C and N elements exist. The Co 2p spectrum of Co-ZIF@CC (Figure 4a) showed typical peaks at 796.1 and 780.5 eV attributed to Co^{2+} $2p_{1/2}$ and $2p_{3/2}$, along with satellite peaks at 802.8 and 786.1 eV. Unlike the single Co^{2+} oxidation state of Co-ZIF@CC, the Co 2p spectrum of CoFe-LDH@Co-ZIF@CC showed the mixed valence state of Co^{2+} (781.8 and 795.9 eV) and Co^{3+} (779.6 and 794.1 eV) [20–24]. This implies that the Co^{2+} cations generated by ZIF can be partially oxidized to Co^{3+} cations, thereby promoting the formation of CoFe-LDH. Upon introducing Fe, the binding energy of Co 2p for CoFe-LDH@Co-ZIF@CC shifted toward the direction of lower binding energy compared with Co-ZIF@CC, suggesting there was electronic transfer between Co and Fe. For the Fe 2p spectrum (Figure 4b), the main fitted peaks at 715.7 and 710.3 eV could be ascribed to Fe $2p_{1/2}$ and $2p_{3/2}$. These different valences are beneficial for electrocatalytic performance due to the electron transfer among them [25,26]. Moreover, the O 1s spectrum (Figure 4c) presented the characteristic peaks of an adsorbed H_2O molecule (532.9 eV), OH^- (531.9 eV) and O^{2-} (531.1 eV) [27–29].

Thus, a small amount of iron oxide inevitably appeared in the sample during the synthesis process due to part of the Fe ion chelate with O^{2-} [30]. The C 1s spectrum (Figure S6) was divided into four peaks, ascribed to C=O (289.9 eV), C-O (286.5 eV), C-N (285.3 eV) and C-C/C=C (284.6 eV), respectively [31]. The N 1s spectrum (Figure S7) displayed its characteristic peaks at 402.9, 401.3, 400.3, 399.2 and 398.5 eV, ascribed to oxidized-N, graphitic-N, pyrrolic-N, $Co-N_x$, and $Fe-N_x$ species. Due to the coexistence of multi-metal, the peak position of $Fe-N_x$ will have a certain deviation in the N 1s spectrum, as reported in the literature [32], but this does not deny the existence of the $Fe-N_X$ locus. Doped nitrogen not only provides active sites for catalysis, but also builds metal-N bonds to allow rapid surface reconstruction in order to enhance the OER catalysis [33–35].
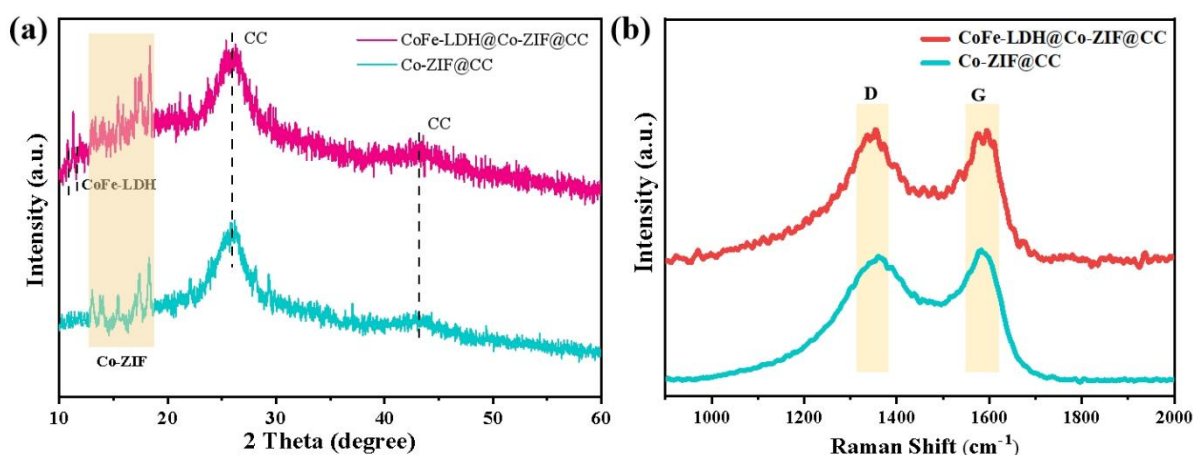
Figure 3. Structural characterization for CoFe-LDH@Co-ZIF@CC and Co-ZIF@CC: (**a**) XRD pattern, (**b**) Raman spectra.

Encouraged by its unique structural advantages, the electrocatalytic OER activity for the CoFe-LDH@Co-ZIF@CC integrated electrode adopted the typical three-electrode system in a strong 1.0 M KOH alkaline solution. In addition, the Co-ZIF@CC and commercial IrO_2 catalysts were also evaluated in the same condition. All the potentials were 95% IR corrected. As displayed in Figure 5a,b, at 10 and 100 mA cm^{-2} current densities, the polarization curves showed that Co-ZIF@CC can deliver the overpotentials of 247 and 393 mV, which are comparable to the commercial IrO_2 (275 and 412 mV). Remarkably, the CoFe-LDH@Co-ZIF@CC possessed the best OER activity at 10 and 100 mA cm^{-2} with the overpotentials of 225 and 319 mV, outperforming a number of reported transition-metal carbon nanomaterial catalysts in recent years (Table S2). From Figure 5c, it can be seen that a Tafel plot based on the polarization curve of CoFe-LDH@Co-ZIF@CC exhibited excellent kinetic performance with the Tafel slope of 81.8 mV dec^{-1}. It was smaller than that of Co-ZIF@CC (166.3 mV dec^{-1}) and IrO_2 (115.2 mV dec^{-1}), indicating that CoFe-LDH@Co-ZIF@CC possesses fast reaction kinetics and outstanding OER catalytic activity. In addition, compared with the powder coated electrode, the self-supported CoFe-LDH@Co-ZIF@CC electrode is obviously superior to many recently reported CoFe bimetallic powder catalysts, as shown in Table S3, which further demonstrates the advantage of the self-supported electrode. EIS measurements were conducted to further study the reaction kinetics of these electrodes. The corresponding Nyquist plots are presented in Figure 5d, with an equivalent circuit shown in the inset. The semicircles of the Nyquist plot on behalf of the charge transfer resistance (R_{ct}), and the smaller semicircles suggest there was a rapid charge transfer at the interface [29]. CoFe-LDH@Co-ZIF@CC exhibited much smaller R_{ct} (9.3 Ω) than Co-ZIF@CC (15.8 Ω), indicating that CoFe-LDH@Co-ZIF@CC possesses robust interfacial electron transfer kinetics and excellent electric conductivity.
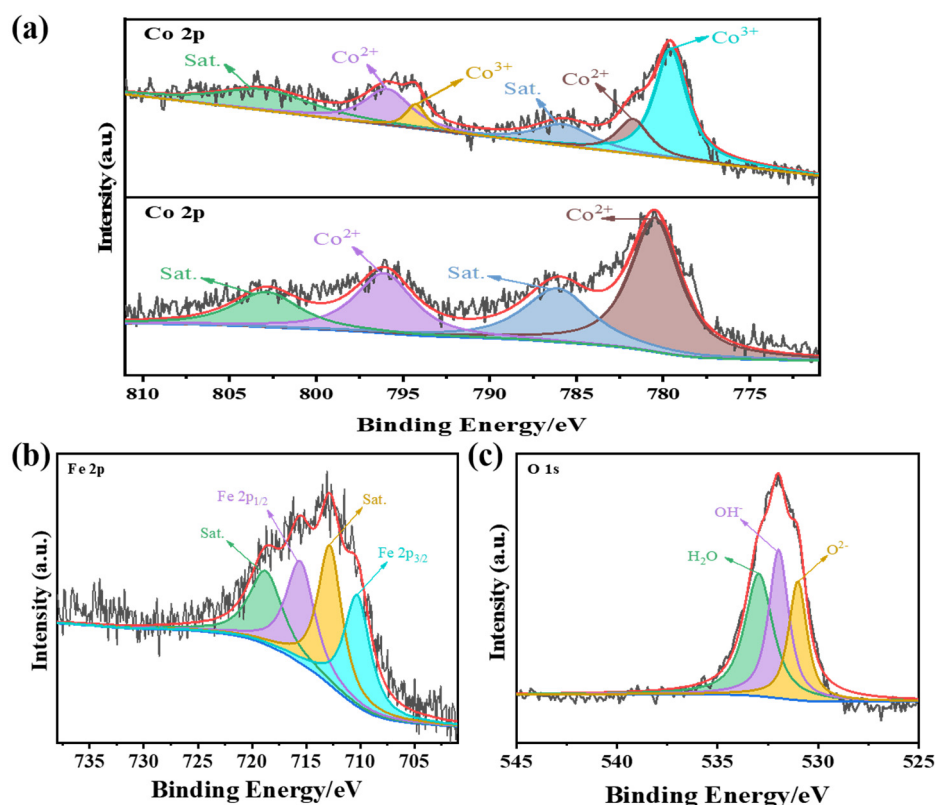
Figure 4. High-resolution XPS spectra of CoFe-LDH@Co-ZIF@CC: (**a**) Co 2p, (**b**) Fe 2p and (**c**) O 1s, respectively.

To further investigate the inherent characteristics that cause such excellent OER catalytic activity, the electrochemical surface area (ECSA) for the abovementioned catalysts was measured through electrochemical double-layer capacitance (C_{dl}). The calculated C_{dl} of CoFe-LDH@Co-ZIF@CC (Figure 5e and Figure S8) was as high as 58.72 mF/cm^2, which was about 2 times larger than that of Co-ZIF@CC (28.71 mF/cm^2). The test data were basically consistent with the fitting line. The higher C_{dl} value of CoFe-LDH@Co-ZIF@CC demonstrates its larger ECSA, indicating there are more active sites for OER after constructing highly ordered hierarchical nanoarrays on self-supported CC. In order to make a complete study of the electrochemical performance, the ECSA was further investigated according to ECSA = $C_{dl}/C_s \times A$. In this circumstance, C_s was 0.04 mFcm^{-2} in a 1.0 M KOH solution, and A indicated the geometric area of the material, which was 1×1 cm = 1 cm^2. At this point, the ECSA of CoFe-LDH@Co-ZIF@CC was calculated as 1554 cm^2, which was superior to that of Co-ZIF@CC (584 cm^2), which is attributable to its larger reaction specific surface area and abundant active sites in this electrochemical reaction system. Combined with Tafel and EIS analysis results, we can conclude that its higher ECSA is the reason for its obvious improvement in OER activity. CoFe-LDH@Co-ZIF@CC also displayed outstanding durability after 30 h in 1.0 M KOH (Figure 5f). After the durability test, the polarization curve of CoFe-LDH@Co-ZIF@CC was close to the initial polarization curve (Figure S9). The SEM image in Figure S10 exhibits the morphological characteristics of CoFe-LDH@Co-ZIF@CC, as after the stability test the anode remained intact.

Under the guidance of the structure–activity relationship, the excellent OER activity for CoFe-LDH@Co-ZIF@CC may be due to the following factors: Firstly, the CC self-supported substrate provides a platform for CoFe-LDH@Co-ZIF to firmly root in CC without the need for additional adhesives, which ensures good electrical contact and mechanical stability. Secondly, well-organized CoFe-LDH@Co-ZIF arrays offer an electron and ion transport channel, facilitating electrolyte penetration and gas release. Thirdly, for CoFe-LDH and Co-ZIF, the synergistic effect creates abundant active sites to enhance catalytic efficiency.
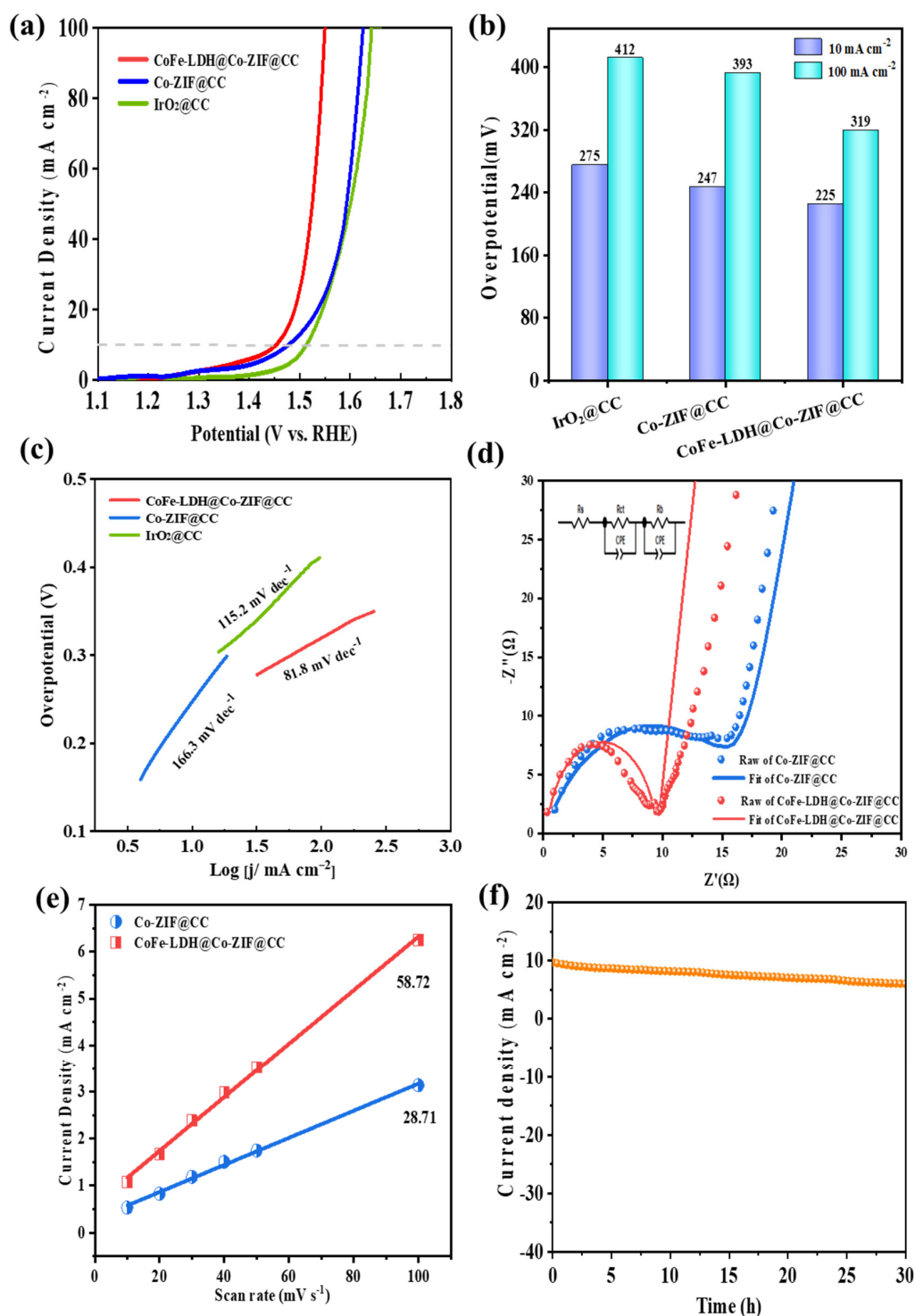
Figure 5. OER of as-prepared catalysts: (**a**) Polarization curves, (**b**) The overpotentials, (**c**) Tafel plots, (**d**) EIS spectra, (**e**) C_{dl} values and (**f**) *i-t* curve of CoFe-LDH@Co-ZIF@CC.

4. Conclusions

In summary, a highly effective electrocatalyst CoFe-LDH@Co-ZIF@CC was fabricated by adopting Co-ZIF as a precursor through ion-exchange/etching reaction with $Fe(NO_3)_3$. The CoFe-LDH@Co-ZIF@CC showed excellent OER electrocatalytic activity for the overpotentials of 225 and 319 mV at 10 and 100 mA cm^{-2} current density, which is comparable to other reported transition-metal carbon nanomaterial catalysts developed in recent years. Benefiting from the synergistic effect between ZIF and LDH, this project provides an attrac-

tive approach for designing catalysts in water splitting. Considering these encouraging results already achieved, future work should be devoted to this research. However, in order to realize industrialization in the field, more in-depth research is needed to solve the following challenges: (1) The synthesis strategy needs to be continuously improved and innovated to prepare more advanced ZIF and LDH composites. (2) The composite structure needs to be further optimized to improve the electrochemical performance of the material. (3) The interaction mechanism between the composition, structure and electrochemical performance of composites should be further explored.

Supplementary Materials: The following are available online at https://www.mdpi.com/article/10.3390/ma15124170/s1, Figure S1. SEM image of CC. Figure S2. SEM image of CoFe-LDH@Co-ZIF@CC. Figure S3. HRTEM images of CoFe-LDH@Co-ZIF@CC. Figure S4. XRD for Co-L-ZIF. Figure S5. XPS survey spectrum of CoFe-LDH@Co-ZIF@CC. Figure S6. XPS C 1s spectrum of CoFe-LDH@Co-ZIF@CC. Figure S7. XPS N 1s spectrum of CoFe-LDH@Co-ZIF@CC. Figure S8. Cyclic voltammograms of (a) CoFe-LDH@Co-ZIF@CC and (b) Co-ZIF@CC with various scan rates (10, 20, 30, 40, 50 and 100 mV/s) in 1.0 M KOH. Figure S9. Polarization curves recorded of CoFe-LDH@Co-ZIF@CC before and after the stability test. Figure S10. SEM image showing CoFe-LDH@Co-ZIF@CC as anode after stability test. Table S1. Contents of elements in CoFe-LDH@Co-ZIF@CC of XPS analysis. Table S2. Comparing OER catalytic performance for CoFe-LDH@Co-ZIF@CC with other reported transition-metal carbon nanomaterial catalysts in recent years. Table S3. OER performance of recently reported CoFe bimetallic powder catalyst. References [36–50] are cited in the supplementary materials.

Author Contributions: Conceptualization, investigation, and writing—original draft, X.D.; data processing, W.Z. and M.Z.; editing, Y.J. and K.S.; funding acquisition and supervision, Z.L. All authors have read and agreed to the published version of the manuscript.

Institutional Review Board Statement: Not applicable.

Informed Consent Statement: Not applicable.

Data Availability Statement: The data presented in this study are available upon request from the corresponding author.

Conflicts of Interest: The authors declare no conflict of interest.

References

1. Gao, Y.Y.; Cui, M.H.; Qu, S.C.; Zhao, H.P.; Shen, Z.T.; Tan, F.R.; Dong, Y.L.; Qin, C.C.; Wang, Z.J.; Zhang, W.F.; et al. Efficient Organic Solar Cells Enabled by Simple Non-Fused Electron Donors with Low Synthetic Complexity. *Small* **2022**, *18*, 2104623–2104632. [CrossRef] [PubMed]
2. Karmakar, A.; Karthick, K.; Sankar, S.S.; Kumaravel, S.; Madhu, R.; Kundu, S. A vast exploration of improvising synthetic strategies for enhancing the OER kinetics of LDH structures: A review. *J. Mater. Chem. A* **2021**, *9*, 1314–1352. [CrossRef]
3. Chen, T.W.; Kalimuthu, P.; Anushya, G.; Chen, S.M.; Mariyappan, V.; Ramachandran, R. Recent Progress in the Development of Advanced Functionalized Electrodes for Oxygen Evolution Reaction: An Overview. *Materials* **2021**, *14*, 4420. [CrossRef] [PubMed]
4. Jin, X.; Li, J.; Xu, T.T.; Cui, Y.T.; Usoltseva, N.; An, V.; Zhang, X.L.; Liu, B.D. Hierarchical Ni2P@NiFe LDH Heterostructural Nanosheet Arrays for Highly Efficient Oxygen Evolution Reaction. *Eur. J. Inorg. Chem.* **2021**, *2021*, 3481–3487. [CrossRef]
5. Dong, Q.B.; Shuai, C.; Mo, Z.L.; Liu, N.J.; Liu, G.G.; Wang, J.; Pei, H.B.; Jia, Q.Q.; Liu, W.T.; Guo, X.D. CeO2 nanoparticles@ NiFe-LDH nanosheet heterostructure as electrocatalysts for oxygen evolution reaction. *J. Solid State Chem.* **2021**, *296*, 121967–121973. [CrossRef]
6. Yang, Y.Y.; Zhou, Q.; Jiao, L.; Yin, Q.; Li, Z.M.; Zhang, Z.Y.; Hu, Z.A. Amorphous heterogeneous NiFe-LDH@Co(OH)(2) supported on nickel foam as efficient OER electrocatalysts. *Ionics* **2022**, *28*, 341–351. [CrossRef]
7. Pan, K.F.; Zhai, Y.Y.; Zhang, J.W.; Yu, K. FeS2/C Nanowires as an Effective Catalyst for Oxygen Evolution Reaction by Electrolytic Water Splitting. *Materials* **2019**, *12*, 3364. [CrossRef]

8. Kamedulski, P.; Lukaszewicz, J.P.; Witczak, L.; Szroeder, P.; Ziolkowski, P. The Importance of Structural Factors for the Electrochemical Performance of Graphene/Carbon Nanotube/Melamine Powders towards the Catalytic Activity of Oxygen Reduction Reaction. *Materials* **2021**, *14*, 2448. [CrossRef]

9. Hu, W.K.; Liu, Q.; Lv, T.X.; Zhou, F.; Zhong, Y.J. Impact of interfacial CoOOH on OER catalytic activities and electrochemical behaviors of bimetallic CoxNi-LDH nanosheet catalysts. *Electrochim. Acta* **2021**, *381*, 138276. [CrossRef]

10. Chen, J.X.; Li, S.J.; Qu, Z.Z.; Li, Z.L.; Wang, D.; Shen, J.L.; Li, Y.B. Study on Oxygen Evolution Reaction Performance of Jarosite/C Composites. *Materials* **2022**, *15*, 668. [CrossRef]

11. Zhao, C.H.; Wei, F.; Lv, H.L.; Zhao, D.K.; Wang, N.; Li, L.G.; Li, N.W.; Wang, X.F. Fe(III) Ions-Assisted Aniline Polymerization Strategy to Nitrogen-Doped Carbon-Supported Bimetallic CoFeP Nanospheres as Efficient Bifunctional Electrocatalysts toward Overall Water Splitting. *Materials* **2021**, *14*, 1473. [CrossRef] [PubMed]

12. Lin, Y.P.; Wang, H.; Peng, C.K.; Bu, L.M.; Chiang, C.L.; Tian, K.; Zhao, Y.; Zhao, J.Q.; Lin, Y.G.; Lee, J.M.; et al. Co-Induced Electronic Optimization of Hierarchical NiFe LDH for Oxygen Evolution. *Small* **2020**, *16*, 2002426–2002434. [CrossRef] [PubMed]

13. Peng, W.; Yang, X.X.; Mao, L.C.; Jin, J.H.; Yang, S.L.; Zhang, J.J.; Li, G. ZIF-67-derived Co nanoparticles anchored in N doped hollow carbon nanofibers as bifunctional oxygen electrocatalysts. *Chem. Eng. J.* **2021**, *407*, 127157–127167. [CrossRef]

14. Milikic, J.; Balciunaite, A.; Sukackiene, Z.; Mladenovic, D.; Santos, D.M.F.; Tamasauskaite-Tamasiunaite, L.; Sljukic, B. Bimetallic Co-Based (CoM, M = Mo, Fe, Mn) Coatings for High-Efficiency Water Splitting. *Materials* **2021**, *14*, 92. [CrossRef] [PubMed]

15. Guzman-Vargas, A.; Vazquez-Samperio, J.; Oliver-Tolentino, M.A.; Ramos-Sanchez, G.; Flores-Moreno, J.L.; Reguera, E. Influence on the Electrocatalytic Water Oxidation of M2+/M3+ Cation Arrangement in NiFe LDH: Experimental and Theoretical DFT Evidences. *Electrocatalysis* **2017**, *8*, 383–391. [CrossRef]

16. Nie, J.H.; Hong, M.; Zhang, X.H.; Huang, J.L.; Meng, Q.; Du, C.C.; Chen, J.H. 3D amorphous NiFe LDH nanosheets electrodeposited on in situ grown NiCoP@NC on nickel foam for remarkably enhanced OER electrocatalytic performance. *Dalton Trans.* **2020**, *49*, 4896–4903. [CrossRef] [PubMed]

17. Xu, J.J.; Zhao, Y.J.; Li, M.Y.; Fan, G.L.; Yang, L.; Li, F. A strong coupled 2D metal-organic framework and ternary layered double hydroxide hierarchical nanocomposite as an excellent electrocatalyst for the oxygen evolution reaction. *Electrochim. Acta* **2019**, *307*, 275–284. [CrossRef]

18. Yang, R.; Zhou, Y.M.; Xing, Y.Y.; Li, D.; Jiang, D.L.; Chen, M.; Shi, W.D.; Yuan, S.Q. Synergistic coupling of CoFe-LDH arrays with NiFe-LDH nanosheet for highly efficient overall water splitting in alkaline media. *Appl. Catal. B-Environ.* **2019**, *253*, 131–139. [CrossRef]

19. Chen, Z.L.; Ha, Y.; Jia, H.X.; Yan, X.X.; Chen, M.; Liu, M.; Wu, R.B. Oriented Transformation of Co-LDH into 2D/3D ZIF-67 to Achieve Co-N-C Hybrids for Efficient Overall Water Splitting. *Adv. Energy Mater.* **2019**, *9*, 1803918–1803930. [CrossRef]

20. Gao, Z.W.; Ma, T.; Chen, X.M.; Liu, H.; Cui, L.; Qiao, S.Z.; Yang, J.; Du, X.W. Strongly Coupled CoO Nanoclusters/CoFe LDHs Hybrid as a Synergistic Catalyst for Electrochemical Water Oxidation. *Small* **2018**, *14*, 1800195–1800202. [CrossRef]

21. Wu, Y.L.; Xiao, Z.X.; Jin, Z.C.; Li, X.Y.; Chen, Y.L. The cobalt carbide/bimetallic CoFe phosphide dispersed on carbon nanospheres as advanced bifunctional electrocatalysts for the ORR, OER, and rechargeable Zn-air batteries. *J. Colloid Interface Sci.* **2021**, *590*, 321–329. [CrossRef] [PubMed]

22. Duan, X.D.; Pan, N.; Sun, C.; Zhang, K.X.; Zhu, X.K.; Zhang, M.D.; Song, L.; Zheng, H.G. MOF-derived Co-MOF,O-doped carbon as trifunctional electrocatalysts to enable highly efficient Zn-air batteries and water-splitting. *J. Energy Chem.* **2021**, *56*, 290–298. [CrossRef]

23. Lei, Z.; Tan, Y.Y.; Zhang, Z.Y.; Wu, W.; Cheng, N.C.; Chen, R.Z.; Mu, S.C.; Sun, X.L. Defects enriched hollow porous Co-N-doped carbons embedded with ultrafine CoFe/Co nanoparticles as bifunctional oxygen electrocatalyst for rechargeable flexible solid zinc-air batteries. *Nano Res.* **2021**, *14*, 868–878. [CrossRef]

24. Dong, G.H.; Lang, K.; Gao, Y.X.; Zhang, W.Z.; Guo, D.X.; Li, J.L.; Chai, D.F.; Jing, L.Q.; Zhang, Z.H.; Wang, Y.Y. A novel composite anode via immobilizing of Ce-doped PbO2 on CoTiO3 for efficiently electrocatalytic degradation of dye. *J. Colloid Interface Sci.* **2022**, *608*, 2921–2931. [CrossRef]

25. Liu, Q.; Liu, X.; Xie, Y.; Sun, F.F.; Liang, Z.J.; Wang, L.; Fu, H.G. N-Doped carbon coating enhances the bifunctional oxygen reaction activity of CoFe nanoparticles for a highly stable Zn-air battery. *J. Mater. Chem. A* **2020**, *8*, 21189–21198. [CrossRef]

26. Jin, W.Y.; Liu, F.; Guo, X.L.; Zhang, J.; Zheng, L.K.; Hu, Y.C.; Mao, J.; Liu, H.; Xue, Y.M.; Tang, C.C. Self-supported CoFe LDH/Co0.85Se nanosheet arrays as efficient electrocatalysts for the oxygen evolution reaction. *Catal. Sci. Technol.* **2019**, *9*, 5736–5744. [CrossRef]

27. Zhao, M.; Guo, T.L.; Qian, W.; Wang, Z.; Zhao, X.; Wen, L.L.; He, D.P. Fe-incorporated cobalt-based metal-organic framework ultrathin nanosheets for electrocatalytic oxygen evolution. *Chem. Eng. J.* **2021**, *422*, 130055–130062. [CrossRef]

28. Wang, Y.Q.; Tao, S.; Lin, H.; Wang, G.P.; Zhao, K.N.; Cai, R.M.; Tao, K.W.; Zhang, C.X.; Sun, M.Z.; Hu, J.; et al. Atomically targeting NiFe LDH to create multivacancies for OER catalysis with a small organic anchor. *Nano Energy* **2021**, *81*, 105606–105617. [CrossRef]

29. Yin, L.L.; Du, X.; Di, C.Z.; Wang, M.W.; Su, K.M.; Li, Z.H. In-situ transformation obtained defect-rich porous hollow CuO@CoZn-LDH nanoarrays as self-supported electrode for highly efficient overall water splitting. *Chem. Eng. J.* **2021**, *414*, 128809–128818. [CrossRef]

30. Wang, Y.; Pan, Y.; Zhu, L.K.; Yu, H.H.; Duan, B.Y.; Wang, R.W.; Zhang, Z.T.; Qiu, S.L. Solvent-free assembly of Co/Fe-containing MOFs derived N-doped mesoporous carbon nanosheets for ORR and HER. *Carbon* **2019**, *146*, 671–679. [CrossRef]

31. Li, G.J.; Tang, Y.B.; Fu, T.T.; Xiang, Y.; Xiong, Z.P.; Si, Y.J.; Guo, C.Z.; Jiang, Z.Q. S, N co-doped carbon nanotubes coupled with CoFe nanoparticles as an efficient bifunctional ORR/OER electrocatalyst for rechargeable Zn-air batteries. *Chem. Eng. J.* **2022**, *429*, 132174–132181. [CrossRef]

32. Gong, L.Y.; Zhang, H.; Wang, Y.; Luo, E.G.; Li, K.; Gao, L.Q.; Wang, Y.M.; Wu, Z.J.; Jin, Z.; Ge, J.J.; et al. Bridge Bonded Oxygen Ligands between Approximated FeN(4)Sites Confer Catalysts with High ORR Performance. *Angew. Chem.-Int. Ed.* **2020**, *59*, 13923–13928. [CrossRef] [PubMed]

33. Li, C.H.; Zhou, E.H.; Yu, Z.Y.; Liu, H.X.; Xiong, M. Tailor-made open porous 2D CoFe/SN-carbon with slightly weakened adsorption strength of ORR/OER intermediates as remarkable electrocatalysts toward zinc-air batteries. *Appl. Catal. B-Environ.* **2020**, *269*, 118771–118780. [CrossRef]

34. Zhang, M.D.; Dai, Q.B.; Zheng, H.G.; Chen, M.D.; Dai, L.M. Novel MOF-Derived Co@N-C Bifunctional Catalysts for Highly Efficient Zn-Air Batteries and Water Splitting. *Adv. Mater.* **2018**, *30*, 1705431–1705440. [CrossRef] [PubMed]

35. Cheng, W.Z.; Liang, J.L.; Yin, H.B.; Wang, Y.J.; Yan, W.F.; Zhang, J.N. Bifunctional iron-phtalocyanine metal-organic framework catalyst for ORR, OER and rechargeable zinc-air battery. *Rare Met.* **2020**, *39*, 815–823. [CrossRef]

36. Huang, K.; Zhang, B.; Wu, J.; Zhang, T.; Peng, D.; Cao, X.; Zhang, Z.; Li, Z.; Huang, Y. Exploring the impact of atomic lattice deformation on oxygen evolution reactions based on a sub-5 nm pure face-centred cubic high-entropy alloy electrocatalyst. *J. Mater. Chem. A* **2020**, *8*, 11938–11947. [CrossRef]

37. Dai, W.; Lu, T.; Pan, Y. Novel and promising electrocatalyst for oxygen evolution reaction based on MnFeCoNi high entropy alloy. *J. Power Sources* **2019**, *430*, 104–111. [CrossRef]

38. Huang, Y.; Chen, X.; Ge, S.; Zhang, Q.; Zhang, X.; Li, W.; Cui, Y. Hierarchical FeCo2S4@CoFe layered double hydroxide on Ni foam as a bifunctional electrocatalyst for overall water splitting. *Catal. Sci. Technol.* **2020**, *10*, 1292–1298. [CrossRef]

39. Li, R.; Li, X.; Liu, C.; Ye, M.; Yang, Q.; Liu, Z.; Xie, L.; Yang, G. Enhanced electron transport through a nanoforest-like structure of CoNi nanoalloy@nitrogen-doped carbon nanotubes for highly efficient catalysis of overall water splitting. *Appl. Surf. Sci.* **2020**, *517*, 145841. [CrossRef]

40. Lu, P.; Chen, X. Nanoscale hetero-structured Co−Co(OH)2 composite/amorphous carbon core/shell bi-functional electrocatalysts electrochemically evolved from metastable hexagonal-phase cobalt for overall water splitting. *Electrochim. Acta* **2021**, *386*, 138517–138524. [CrossRef]

41. Li, R.; Li, X.; Yu, D.; Li, L.; Yang, G.; Zhang, K.; Ramakrishna, S.; Xie, L.; Peng, S. Ni3ZnC0.7 nanodots decorating nitrogen-doped carbon nanotube arrays as a self-standing bifunctional electrocatalyst for water splitting. *Carbon* **2019**, *148*, 496–503. [CrossRef]

42. Liu, S.L.; Wan, R.D.; Lin, Z.S.; Liu, Z.; Liu, Y.G.; Tian, Y.; Qin, D.D.; Tang, Z.H. Probing the Co role in promoting the OER and Zn-air battery performance of NiFe-LDH: A combined experimental and theoretical study. *J. Mater. Chem. A* **2022**, *10*, 5244–5254. [CrossRef]

43. Shamloofard, M.; Shahrokhian, S.; Amini, M.K. Mesoporous nanostructures of NiCo-LDH/ZnCo(2)O4 as an efficient electrocatalyst for oxygen evolution reaction. *J. Colloid Interface Sci* **2021**, *604*, 832–843. [CrossRef] [PubMed]

44. Yuan, F.F.; Zhang, E.L.; Liu, Z.H.; Yang, K.; Zha, Q.Q.; Ni, Y.H. Hollow CoSx Nanoparticles Grown on FeCo-LDH Microtubes for Enhanced Electrocatalytic Performances for the Oxygen Evolution Reaction. *Acs Appl. Energy Mater.* **2021**, *4*, 12211–12223. [CrossRef]

45. Elbakkay, M.H.; El-Dek, S.I.; Farghali, A.A.; Rouby, W. Highly active atomic Cu catalyst anchored on superlattice CoFe layered double hydroxide for efficient oxygen evolution electrocatalysis. *Int. J. Hydrog. Energy* **2022**, *47*, 9876–9894. [CrossRef]

46. Li, M.; Gu, Y.; Chang, Y.J.; Gu, X.C.; Tian, J.Q.; Wu, X.; Feng, L.G. Iron doped cobalt fluoride derived from CoFe layered double hydroxide for efficient oxygen evolution reaction. *Chem. Eng. J.* **2021**, *425*. [CrossRef]

47. Wang, B.; Hu, Y.; Yu, B.; Zhang, X.J.; Yang, D.X.; Chen, Y.F. Heterogeneous CoFe-Co8FeS8 nanoparticles embedded in CNT networks as highly efficient and stable electrocatalysts for oxygen evolution reaction. *J. Power Sources* **2019**, *433*. [CrossRef]

48. Wang, B.; Zhou, L.L.; Huang, Z.Q.; Pan, D.S.; Guo, Z.H.; Song, J.L. In situ construction of N-doped amorphous CoFe selenites toward efficient electrocatalytic water oxidation. *J. Power Sources* **2021**, *483*. [CrossRef]

49. Pan, D.S.; Chen, P.; Zhou, L.L.; Liu, J.H.; Guo, Z.H.; Song, J.L. Self-template construction of 2D amorphous N-doped CoFe-mesoporous phosphate microsheets for zinc-air batteries. *J. Power Sources* **2021**, *498*. [CrossRef]

50. Hao, C.Y.; Wu, Y.; An, Y.J.; Cui, B.H.; Lin, J.N.; Li, X.N.; Wang, D.H.; Jiang, M.H.; Cheng, Z.X.; Hu, S. Interface-coupling of CoFe-LDH on MXene as high-performance oxygen evolution catalyst. *Mater. Today Energy* **2019**, *12*, 453–462. [CrossRef]